Research Square

Preprints are preliminary reports that have not undergone peer review.
They should not be considered conclusive, used to inform clinical practice,
or referenced by the media as validated information.

High hydrostatic pressure pretreatment enhances quercetin-mediated attenuation of wheat gliadin immunoreactivity and FcεRI signaling

Weiman Gao
Beijing Forestry University
Lining Ren
Beijing Forestry University
Xinyu Ma
Beijing Forestry University
Yuhang Xiao
Beijing Forestry University
Shijing Jiang
Beijing Forestry University
Aidong Sun
adsun@bjfu.edu.cn

Beijing Forestry University

Article

Keywords: Wheat gliadin, Quercetin, High hydrostatic pressure, B-cell epitopes, KU812 cells, FcεRI signaling

Posted Date: November 13th, 2026

DOI: https://doi.org/10.21203/rs.3.rs-11163978/v1

License: This work is licensed under a Creative Commons Attribution 4.0 International License.
Read Full License

Additional Declarations: No competing interests reported.

High hydrostatic pressure pretreatment enhances quercetin-mediated attenuation of wheat gliadin immunoreactivity and FcεRI signaling

Weiman Gao[a,b], Lining Ren[a,b], Xinyu Ma[a,b], Yuhang Xiao[a,b], Shijing Jiang[a,b], Aidong Sun[a,b*]

[a]*Department of Food Science and Engineering, College of Biological Sciences and Biotechnology, Beijing Key Laboratory of Forest Food Processing and Safety, Beijing Forestry University, Beijing 100083, China*

[b]*Hebei Province Key Laboratory of Sustainable Utilization and Development of Forest Food Resources, Beijing Forestry University, Beijing 100083, China*

Corresponding author: Aidong Sun; E-mail: adsun@bjfu.edu.cn

College of Biological Sciences and Biotechnology,

Beijing Forestry University, No. 35, Qinghua East Road, Beijing, China.

Abstract

Gliadin is a major trigger of allergic responses to wheat-based products. Although previous studies have shown that polyphenol intervention or physical modification can attenuate its immunoreactivity, the combined effects of polyphenols and high hydrostatic pressure (HHP) on this property remain poorly understood, and the optimal processing order is unclear. In this study, quercetin (Que) and 500 MPa HHP were initially selected as the most effective polyphenol and pressure conditions based on IgE-binding assays. Notably, HHP pretreatment followed by Que supplementation led to a significantly greater reduction in IgE-binding capacity than either treatment alone or the reverse sequence, while also sustaining stronger inhibitory effects following simulated gastrointestinal digestion. Structural characterization and molecular dynamics simulations further revealed that HHP pretreatment facilitated Que binding to gliadin through conformational relaxation and surface remodeling, resulting in lower conformational flexibility, a more robust interaction network, and the most favorable binding free energy (−20.18 ± 3.17 kcal/mol). Additionally, peptide-level mass spectrometry analysis identified 27 putative linear B-cell epitope-containing peptides, 21 of which exhibited reduced abundance in the Gli-HHP-Que group, while several responsive peptides mapped near the predicted Que-binding region. Consistently, Gli-HHP-Que most effectively suppressed Ca^{2+} mobilization, degranulation, and inflammatory mediator release in serum-sensitized KU812 cells, together with reduced activation of the FcεRI-associated Lyn/Syk/PLCγ1 axis and downstream MAPK/NF-κB signaling. Collectively, these

findings elucidate the mechanistic basis by which combined HHP and polyphenol treatment modulates gliadin immunoreactivity, and propose a feasible combinatorial processing strategy for reducing the allergenicity of wheat-based products.

Keywords: Wheat gliadin; Quercetin; High hydrostatic pressure; B-cell epitopes; KU812 cells; FcεRI signaling.

1 Introduction

Wheat is one of the most widely consumed cereal crops worldwide; however, its proteins can elicit adverse immune reactions in susceptible individuals. Wheat allergy is a typical IgE-mediated food allergy that can manifest as atopic dermatitis, urticaria, gastrointestinal symptoms, wheat-dependent exercise-induced anaphylaxis (WDEIA), or even life-threatening anaphylactic shock, thereby posing a substantial challenge to dietary safety and quality of life [1]. Among wheat proteins, gliadin is particularly relevant because of its high glutamine and proline contents, repetitive sequence regions, and relative resistance to gastrointestinal digestion, making it one of the major contributors to wheat allergenicity [2,3]. Multiple α/β-, γ-, and ω-gliadin components contain IgE-binding epitopes, and their glutamine- and proline-rich linear sequences are closely associated with serum IgE recognition in patients with wheat allergy [4]. Therefore, reducing the accessibility, digestive persistence, and immune recognition of gliadin epitopes through food-processing approaches represents an important strategy for decreasing gliadin immunoreactivity.

Food-processing technologies have been widely used to modulate protein immunoreactivity by inducing conformational remodeling, aggregation or cross-linking, changes in digestive susceptibility, and alteration of linear or conformational epitope accessibility [5-7]. High hydrostatic pressure (HHP) processing is a promising non-thermal technology for modulating food protein allergenicity. By disrupting weak non-covalent interactions, HHP can alter higher-order protein structures, aggregation behavior, and immunoreactivity while largely preserving

nutritional and sensory quality. For example, pressure-induced conformational remodeling has been reported to increase protein susceptibility to gastrointestinal digestion and reduce IgE-binding capacity by modifying the exposure of epitope-related regions [8]. However, the effects of HHP are dependent on pressure intensity and protein structure; pressure-induced unfolding may either reduce epitope accessibility or promote reaggregation and re-exposure of previously buried regions. Moreover, because HHP primarily modifies non-covalent interactions and higher-order structure, it may have limited ability to alter stable linear epitope sequences when applied alone. In wheat gluten systems, HHP has been reported to induce the release and conformational rearrangement of allergenic proteins, which may create a more accessible conformational state for subsequent modification [9,10].

Apart from physical processing, protein-polyphenol interactions have also been widely explored as an effective strategy for modulating food protein allergenicity. Polyphenols can interact with allergenic proteins through hydrogen bonding, hydrophobic interactions, van der Waals forces, π-π stacking, or oxidation-induced covalent binding, thereby inducing conformational remodeling, aggregation or cross-linking, altered digestive susceptibility, and masking or disruption of IgE-recognized epitopes. [7,11]. This strategy has been applied to several food allergens, including soybean, peanut, milk, egg, and plant-derived allergens, where polyphenol-mediated modification reduced IgE-binding capacity [12-14]. More recent studies further showed that tannin-rich chestnut inner skin and young persimmon fruit powders decreased allergen signals in processed wheat products, while chlorogenic

88 acid and luteolin conjugation altered gliadin conformation and reduced IgE/IgG
89 binding capacity [15,16]. These findings indicate that polyphenol-mediated modification
90 is a feasible approach for reducing wheat protein immunoreactivity.

91 Previous studies have shown that both HHP processing and polyphenol
92 modification can reduce food protein immunoreactivity by altering protein
93 conformation, aggregation behavior, digestive susceptibility, and epitope exposure [8,17].
94 However, most studies have evaluated these two strategies separately, whereas limited
95 attention has been paid to their combined application in allergenic protein
96 modification. When a dual-modification strategy is used, several factors may
97 determine its effectiveness, including the type of polyphenol, pressure intensity, and
98 the sequence in which HHP and polyphenol treatment are applied. In particular,
99 processing order may influence whether the polyphenol interacts with native gliadin
100 or with a pressure-remodeled structure, thereby affecting binding-site accessibility,
101 complex formation, digestive behavior, and epitope availability [18,19]. Moreover,
102 changes in overall IgE-binding capacity alone are insufficient to clarify whether
103 specific linear epitopes are altered.

104 Based on these considerations, this study systematically evaluated the effects of
105 different HHP-polyphenol treatment sequences on the immunoreactivity of wheat
106 gliadin. Different polyphenols and pressure levels were first screened to determine
107 suitable modification conditions, after which HHP followed by quercetin treatment
108 was compared with the reverse sequence. Structural and physicochemical
109 characterization and simulated gastrointestinal digestion were used to assess protein

remodeling, dispersion behavior, digestive susceptibility, and post-digestion IgE-binding capacity. Molecular docking and molecular dynamics simulations were further performed to clarify how treatment sequence affected gliadin-quercetin binding behavior and complex stability. In addition, putative linear B-cell epitope-containing peptides were screened by integrating in silico prediction with LC-MS/MS-based peptide identification and were subsequently quantified by parallel reaction monitoring. Finally, serum-sensitized KU812 cells were used to determine whether the selected processing sequence attenuated IgE-dependent cellular activation and FcεRI-associated signaling. This study aimed to establish the relationship among treatment sequence, gliadin structural remodeling, protein-polyphenol interactions, digestive immunoreactivity, epitope-associated peptide responses, and cellular activation, thereby providing a scientific basis for designing non-thermal processing strategies for wheat protein ingredients with reduced allergenic potential.

2 Materials and methods

2.1 Chemicals and reagents

Wheat gliadin was purchased from Shanghai Macklin Biochemical Co., Ltd. Quercetin, catechin, caffeic acid, chlorogenic acid, and other polyphenol standards were purchased from Beijing Solarbio Science & Technology Co., Ltd. (Beijing, China). IRT standard peptides were purchased from Biognosys and used for signal correction in PRM quantification. C18 desalting columns were used for purification and desalting of digested peptides. All other reagents were of analytical grade.

2.2 Human sera

Sera from 5 clinically diagnosed wheat-allergic patients were commercially obtained from PlasmaLab International (USA). All positive sera showed detectable wheat-specific IgE (sIgE), with levels ranging from 15.2 to 52.8 kU/L. Detailed information on the demographic characteristics, clinical symptoms, and wheat-specific sIgE levels of the wheat-allergic patients is provided in Table S1. Serum from healthy individuals was used as the negative control. Before use, positive sera were pooled in equal volumes to minimize inter-individual variation.

2.3 Preparation of gliadin-polyphenol complexes

Gliadin-polyphenol complexes were prepared using an alkaline treatment method. Briefly, wheat gliadin and polyphenol standards were separately dissolved in 70% ethanol solution, and the pH was adjusted to 9.0 using NaOH. The two solutions were then mixed at an equal volume to obtain final concentrations of 5 μmol/L gliadin and 30 μmol/L polyphenols. The mixture was stirred magnetically at room temperature under light-shielding conditions for 4 h. After reaction, the samples were dialyzed against 70% ethanol for 12 h to remove free polyphenols. Ethanol was subsequently removed by rotary evaporation, and the samples were freeze-dried to obtain gliadin-polyphenol complexes.

2.4 HHP processing of gliadin

Gliadin solution was prepared at a concentration of 1 mg/mL. An appropriate volume of the solution was packed into pressure-resistant bags, vacuum-sealed, and then subjected to high-pressure processing. The pressure levels were set at 100, 200, 300, 400, 500, and 600 MPa, with a holding time of 20 min. Untreated gliadin solution was used as the control.

For the combined treatment groups, Gli-HHP-Que refers to gliadin first treated by high pressure at 500 MPa and then reacted with quercetin, whereas Gli-Que-HHP refers to gliadin first complexed with quercetin and then subjected to HHP treatment at 500 MPa.

2.5 Indirect ELISA analysis of IgE-binding capacity

The IgE-binding capacity of different treated samples was evaluated by indirect ELISA. Samples were diluted to 4 μg/mL with coating buffer, and 100 μL of each sample was added to each well of a microplate, followed by overnight coating at 4 °C. After discarding the coating solution, the wells were washed three times with PBST and blocked with 1% BSA at 37 °C for 1 h. After washing, 100 μL of diluted antiserum was added to each well. The allergic patient serum and negative serum were serially diluted with PBS at a ratio of 1:20 and incubated at 37 °C for 1 h. Healthy-donor serum diluted in the same manner was used as the negative-serum control. Subsequently, 100 μL of HRP-conjugated goat anti-human IgE secondary antibody was added to each well and incubated. After washing, TMB substrate solution was added and reacted in the dark at 37 °C for 15 min. The reaction was

terminated with 2 mol/L H_2SO_4, and the absorbance was measured at 450 nm. Relative IgE-binding reduction was calculated as follows:

$$\text{Relative IgE-binding reduction (\%)} = 1 - \frac{OD_{sample}}{OD_{\text{native gliadin}}} \times 100$$

2.6 SDS-PAGE

SDS-PAGE was performed to analyze the molecular weight distribution of native and treated gliadin samples. The protein concentration was adjusted to 1 mg/mL and mixed with 4×loading buffer at a ratio of 3:1. The samples were denatured at 95 °C for 10 min and separated using a 10% polyacrylamide gel. After electrophoresis, the gel was stained with Coomassie Brilliant Blue R-250 and destained sufficiently to observe and record the protein band patterns.

2.7 Circular dichroism spectroscopy

Circular dichroism spectroscopy was used to analyze the effects of different treatments on the secondary structure of gliadin. The treated samples were diluted to 0.2 mg/mL, and 200 μL of each sample was transferred into a quartz cuvette with a path length of 0.5 mm. Spectra were recorded from 190 to 250 nm under continuous nitrogen flushing. The scanning parameters were set as follows: step size, 1 nm; scanning time per point, 2 s; and two repeated scans for each sample. The obtained spectra were baseline-corrected and smoothed before comparative analysis.

2.8 Intrinsic fluorescence spectroscopy

198 Intrinsic fluorescence spectroscopy was used to analyze changes in the
199 microenvironment of aromatic amino acid residues in gliadin. Different treated
200 samples were prepared at 0.2 mg/mL in 70% ethanol solution, and 1 mL of each
201 sample was transferred into a fluorescence cuvette. Fluorescence spectra were
202 recorded using a fluorescence spectrophotometer with an excitation wavelength of
203 285 nm and an emission wavelength range of 300-500 nm. Both excitation and
204 emission slit widths were set at 5.0 nm.
205
206 **2.9 UV-visible spectroscopy**
207 Using 70% ethanol solution as the blank reference, UV-visible absorption
208 spectra of different treated gliadin samples were recorded over the range of 200-500
209 nm using a UV-Vis spectrophotometer. The sample concentration was 0.2 mg/mL.
210
211 **2.10 Particle size and zeta potential**
212 The particle size and zeta potential of different treated samples were determined
213 using a Nano-ZS 90 Malvern particle size analyzer. Briefly, 1 mL of each sample was
214 transferred into the sample cell and measured using a He/Ne laser. The refractive
215 indices of protein particles and the dispersion medium were set to 1.46 and 1.33,
216 respectively. For zeta potential measurement, samples were equilibrated for 60 s
217 before detection, and at least 14 consecutive readings were recorded for each sample.
218 All measurements were performed at room temperature in triplicate.
219

220 **2.11 Free sulfhydryl content**

221 The free sulfhydryl content was determined using Ellman's reagent. Briefly,
222 0.015 g of protein sample was dissolved in 5 mL of Tris-glycine buffer and incubated
223 at 25 °C for 1 h. DTNB solution was then added, and the mixture was incubated in the
224 dark for 15 min. The mixture was centrifuged at 10,000 × g for 15 min at 4 °C, and
225 the absorbance of the supernatant was measured at 412 nm. Buffer instead of protein
226 solution was used as the reagent blank, while buffer instead of DTNB solution was
227 used as the protein blank. The free sulfhydryl content was calculated as follows:

228 $$SHF=73.53 \times A_{412} \times \frac{D}{C}$$

229 where A_{412} is the absorbance at 412 nm, D is the dilution factor, and C is the
230 protein concentration.

231

232 **2.12 Surface hydrophobicity**

233 The surface hydrophobicity of the samples was determined using the ANS
234 fluorescent probe method. Briefly, 20 μL of ANS solution was mixed with 4 mL of
235 different treated gliadin solutions and incubated in the dark for 20 min. The mixture
236 was then centrifuged at 5000 × g for 5 min at 4 °C. The supernatant was collected,
237 and the protein concentrations of all samples were adjusted to the same level.
238 Fluorescence intensity was measured using a fluorescence spectrophotometer with an
239 excitation wavelength of 375 nm and an emission wavelength range of 430-610 nm.
240 Subtract the fluorescence intensity of the ANS solution (without the sample) from the
241 fluorescence intensity of the sample. Calculate the H_0 index by determining the initial

242 slope of the curve relating fluorescence intensity to protein concentration.

243

244 **2.13 In vitro simulated gastrointestinal digestion**

245 **2.13.1 Simulated gastric and intestinal digestion**

246 In vitro simulated digestion was performed according to the standardized
247 INFOGEST static model with slight modifications [20]. Protein samples were mixed
248 with pepsin in simulated gastric fluid (SGF), and the pH was adjusted to 3.0 using 1
249 M HCl. The final protein concentration was 2 mg/mL, and the pepsin activity was
250 maintained at 2000 U/mL. The samples were incubated at 37 °C under continuous
251 shaking for 15, 30, 60, 90, and 120 min. Gastric digestion was terminated by
252 sequentially shifting the pH to 7.0 via the addition of simulated intestinal fluid (SIF)
253 containing trypsin and bile salts. For downstream intestinal digestion, the trypsin
254 activity was adjusted to 100 U/mL, and the mixture was incubated at 37 °C for an
255 additional 15, 30, 60, 90, and 120 min. After the designated digestion intervals, the
256 aliquots were immediately heated at 95 °C for 10 min to completely inactivate the
257 enzymes and stored at −20 °C until further analysis.

258 **2.13.2 IgE-binding capacity of digestion products**

259 The ELISA test was conducted using indirect ELISA, and the method was based
260 on that described in Section 2.5.

261 **2.13.3 Determination of degree of hydrolysis**

262 The degree of hydrolysis (DH) of digested gliadin samples was determined using
263 the OPA method with slight modifications. The OPA reagent was prepared by

dissolving 80 mg OPA in 2 mL anhydrous ethanol, followed by the addition of 60 mL 0.3 mol/L sodium tetraborate buffer, 100 mg SDS, and 80 mg DTT, and the final volume was adjusted to 100 mL with deionized water.

Briefly, 400 μL of appropriately diluted sample or L-serine standard solution was mixed with 4 mL OPA reagent and reacted at room temperature for 2 min. The absorbance was then measured at 340 nm. L-serine solutions ranging from 0 to 1.0 mmol/L were used to establish the standard curve. The DH was calculated as follows:

$$DH\ (\%)=\frac{(\frac{C\times V\times 600}{m}-0.4)}{8.8}\times 100$$

where C is the L-serine equivalent concentration calculated from the standard curve (mmol/L), V is the volume of hydrolysate (L), and m is the protein mass in the sample (g).

2.14 Molecular docking and molecular dynamics simulations

2.14.1 Molecular docking

AutoDock Vina was used to analyze the binding mode between gliadin and quercetin. The amino acid sequence of wheat α-gliadin (UniProt ID: P04726) was obtained from the UniProt database, and its three-dimensional structure was constructed using the I-TASSER platform. The three-dimensional structure of quercetin was downloaded from the PubChem Compound Database and energy-minimized. Before docking, water molecules and irrelevant small molecules were removed from the protein structure using PyMOL. AutoDockTools 1.5.6 was then used to add hydrogen atoms, calculate Gasteiger charges, merge nonpolar

hydrogens, and convert the receptor and ligand structures into pdbqt format.

As gliadin lacks a clearly defined active binding pocket, a blind docking strategy was adopted by setting the docking box to cover the entire protein structure, allowing a comprehensive search for potential quercetin-binding sites on the protein surface. During docking, quercetin was treated as a flexible ligand, while the receptor protein was kept rigid. The exhaustiveness and energy_range parameters in AutoDock Vina were set to 100 and 5, respectively, and the top 20 candidate conformations with lower binding energies were retained. Representative conformations were selected based on binding energy, spatial rationality, and protein-ligand interaction characteristics for subsequent molecular dynamics simulations.

2.14.2 Molecular dynamics simulations

Molecular dynamics (MD) simulations of gliadin-quercetin complexes were performed using GROMACS. To accurately capture the experimental treatment sequences, three computational simulation workflows were constructed: Gli-Que, Gli-HHP-Que, and Gli-Que-HHP. Gli-Que represents native gliadin docked with quercetin and simulated under ambient pressure (0.1 MPa) for 200 ns. To simulate the Gli-HHP-Que sequence, the native gliadin structure was first subjected to an independent 200 ns MD simulation under an ultra-high pressure environment of 500 MPa to induce conformational loosening and unfolding; the representative distorted conformation was then extracted from the high-pressure trajectory, returned to ambient pressure (0.1 MPa), and utilized as the modified receptor for quercetin docking, followed by a standard 200 ns ambient production simulation. For

Gli-Que-HHP, the ambient-docked gliadin-quercetin complex was first subjected to a 200 ns simulation under 500 MPa, and then equilibrated back at 0.1 MPa for a 200 ns production simulation.

Each system was placed in a periodic water box, solvated using the TIP3P water model, and neutralized by adding Na^+ or Cl^- ions. Protein parameters were described using the AMBER99SB-ILDN force field, while the topology parameters of quercetin were generated using the GAFF force field through ACPYPE. After energy minimization, each system was equilibrated under NVT and NPT ensembles and then subjected to production MD simulations. The simulation time was 200 ns with a time step of 2 fs. Long-range electrostatic interactions were treated using the PME method. Trajectories were analyzed using built-in GROMACS tools, including RMSD, RMSF, Rg, and hydrogen bond analyses, to evaluate conformational stability and intermolecular interactions.

In addition, free energy landscape analysis was performed to compare the stable conformational distribution of different systems. The binding free energy of gliadin-quercetin complexes was calculated using gmx_MMPBSA. The binding free energy was further decomposed into van der Waals interaction energy, electrostatic interaction energy, polar solvation energy, and nonpolar solvation energy. Residue energy contribution analysis was conducted to identify key amino acid residues involved in stabilizing quercetin binding. Finally, Discovery Studio Visualizer was used to visualize protein-ligand interactions.

2.15 In silico prediction, identification, and targeted quantification of putative putative linear B-cell epitope-containing peptides by LC-MS/MS and PRM

Representative amino acid sequences of different gliadin subclasses were retrieved from the UniProt database, including ω-5-gliadin (Q402I5), ω-2-gliadin (Q9FUW7), γ-gliadins (A0A060N479 and P08453), and α/β-gliadins (P04725 and D2T2K3). Because γ- and α/β-gliadins comprise multiple homologous isoforms with considerable sequence variation, two representative UniProt sequences were included for each subclass to improve sequence coverage and reduce the possibility of omitting potential epitope regions. Potential linear B-cell epitope regions in these gliadin sequences were predicted using BepiPred 3.0, ABCpred, the B-cell epitope prediction tools available through the Immune Epitope Database and Analysis Resource (IEDB), and the Immunomedicine Group prediction server [21-23]. Sequence-based antigenicity-related profiles, including hydrophilicity, flexibility, surface accessibility, and antigenic propensity, were additionally evaluated using the Protean module of DNASTAR. The default parameters and thresholds of the respective prediction tools were used. The predicted epitope regions generated by the different tools were integrated to establish an in silico candidate epitope library. Detailed information on the gliadin subclasses, UniProt accession numbers, peptide positions, and candidate peptide sequences is provided in Table S2.

For each sample, 180 μg of protein was dissolved in 6 M urea, followed by reduction with TCEP and alkylation with IAA. The sample was then equally divided into three aliquots and digested with trypsin, chymotrypsin, and Glu-C, respectively.

Trypsin and Glu-C digestion were performed in 50 mM NH_4HCO_3 at 37 °C for 16 h, while chymotrypsin digestion was carried out in buffer containing 10 mM $CaCl_2$ and 100 mM Tris-HCl at 30 °C for 16 h. After digestion, peptide solutions derived from the same sample were pooled, desalted using C18 desalting columns, mixed with equal amounts of iRT standard peptides, lyophilized, and stored at −80 °C until analysis

Peptide identification was performed using a Dionex UltiMate 3000 UHPLC system coupled to a Q Exactive mass spectrometer. Peptides were separated on a C18 reversed-phase column using 0.1% formic acid in water and 0.1% formic acid in acetonitrile as mobile phases at a flow rate of 600 nL/min. MS data were acquired in data-dependent acquisition mode. Full MS scans were collected over the m/z range of 300-1400 at a resolution of 70,000. MS/MS spectra were acquired using HCD fragmentation at a resolution of 17,500 and a collision energy of 27, and the top 20 most intense precursor ions were selected for fragmentation.

Raw data were analyzed using Proteome Discoverer 2.1 software against the Triticum aestivum protein database from UniProt. Carbamidomethylation of cysteine was set as a fixed modification, while protein N-terminal acetylation, methionine oxidation, and deamidation of asparagine and glutamine were set as variable modifications. A target-decoy search strategy was used to control the reliability of peptide identification, and the FDR was set to less than 1% at both peptide and protein levels. The peptide sequences confidently identified by DDA LC-MS/MS were mapped to their corresponding gliadin sequences and compared with the in

374 silico-predicted epitope regions. Peptides that matched, were located within,
375 completely contained, or overlapped with the predicted regions were retained as
376 putative epitope-containing peptides. Thus, only peptides jointly supported by in
377 silico prediction and experimental LC-MS/MS identification were considered for
378 subsequent PRM quantification.

379 Targeted quantification of allergenic epitope-containing peptides was performed
380 in PRM mode using the same LC-MS platform and chromatographic conditions
381 described above. iRT standard peptides were included in the scheduled acquisition list
382 for signal correction. A total of 43 precursor ions were targeted and monitored within
383 a retention-time window of ±5 min. Each sample was analyzed in triplicate. PRM data
384 were processed using Skyline 24.1 software for peak area extraction and quantitative
385 analysis. For quantification, the precursor charge state with higher signal intensity and
386 its corresponding b/y fragment ions were selected. In total, 151 fragment ions
387 corresponding to 27 allergenic epitope-containing peptides were used for peak
388 area-based statistical analysis.

389 **2.16 KU812 cell model and evaluation of allergenic activity**

390 **2.16.1 Cell culture and passive sensitization**

391 KU812 cells were cultured in RPMI 1640 medium supplemented with 10% fetal
392 bovine serum and 1% penicillin-streptomycin at 37 °C with 5% CO_2. Cells in the
393 logarithmic growth phase were seeded into 12-well plates at 2×10^6 cells/mL, with 1
394 mL per well. For passive sensitization, cells were incubated with 50 μL of pooled
395 serum from wheat-allergic patients at 37 °C for 24 h. Subsequently, cells were

stimulated for 4 h by adding 50 μL of various gliadin variants (Gli, Gli-Que, Gli-HHP, and Gli-HHP-Que) at a stock concentration of 0.6 mg/mL. Cells treated with healthy control serum and PBS served as the negative control, while those sensitized and challenged with native gliadin served as the model group. After stimulation, cell suspensions were centrifuged at 1000 × g for 5 min. Supernatants were collected for mediator analysis, and cells were harvested for intracellular and protein analyses.

2.16.2 Cell viability assay

Cell viability was evaluated using a commercial CCK-8 kit to determine non-cytotoxic working concentrations. KU812 cells were seeded into 96-well plates and exposed to various concentrations of gliadin samples for 24 h. After adding the CCK-8 reagent and incubating for an additional 2 h, the absorbance was measured at 450 nm using a microplate reader. Relative cell viability was calculated to select appropriate concentrations for subsequent experiments.

2.16.3 Intracellular Ca^{2+} mobilization

Changes in intracellular Ca^{2+} levels in KU812 cells were detected by flow cytometry. Cells in the logarithmic growth phase described in Section 2.16.1 were collected by centrifugation at 1000 × g for 5 min at 4 °C. After removal of the supernatant, the cells were washed twice with PBS and incubated with diluted Fluo-3 AM staining solution at 37 °C for 1 h. The cells were then centrifuged again at 1000 × g for 5 min at 4 °C, washed three times with PBS, and immediately analyzed by flow cytometry.

2.16.4 Degranulation assessment

KU812 cell degranulation was quantified by determining β-hexosaminidase and

418 histamine release, alongside morphological observation. Briefly, the
419 β-hexosaminidase activity in the supernatant was measured using
420 p-nitrophenyl-N-acetyl-β-D-glucosaminide as the substrate at 405 nm, with total
421 enzyme release quantified by lysing cells with 0.5% Triton X-100. Simultaneously,
422 the histamine concentration in the culture supernatant was determined using a
423 commercial ELISA kit. Additionally, for morphological evaluation, treated cells were
424 stained with neutral red working solution, and degranulation morphology was
425 visualized under an inverted microscope to calculate the percentage of degranulated
426 cells.

427 **2.16.5 Western blot analysis**

428 Western blotting was performed to detect the expression of Lyn/Syk/PLCγ1, MAPK,
429 and NF-κB signaling pathway-related proteins. After sample treatment, KU812 cells
430 were collected and lysed using protein lysis buffer. The total protein concentration
431 was measured using the BCA method. Equal amounts of protein were separated by
432 SDS-PAGE and transferred onto PVDF membranes. After blocking, the membranes
433 were incubated with primary antibodies against Lyn, p-Lyn, Syk, p-Syk, PLCγ1,
434 p-PLCγ1, ERK, p-ERK, JNK, p-JNK, p38, p-p38, NF-κB p65, p-NF-κB p65, and
435 β-actin. The membranes were then incubated with HRP-conjugated secondary
436 antibodies and visualized using ECL chemiluminescence. Band intensities were
437 quantified using image analysis software. Target protein expression was normalized
438 to β-actin, and phosphorylated protein levels were normalized to their corresponding
439 total proteins.

2.17 Statistical analysis

All experiments were performed at least in triplicate, and data are presented as the mean ± standard deviation. Statistical analysis was performed using SPSS software. Differences among groups were analyzed by one-way analysis of variance followed by Duncan's multiple comparison test. A value of $p < 0.05$ was considered statistically significant.

3 Results and discussion

3.1 Establishing the treatment conditions and sequence-dependent IgE response of gliadin

Indirect ELISA was performed to evaluate the IgE-binding capacity of gliadin after treatment with different polyphenols. As shown in Fig. 1A, the type of polyphenol significantly influenced the reduction in IgE binding. Among the four polyphenols tested, namely quercetin (Que), chlorogenic acid (CGA), caffeic acid (CA), and catechin (Cat), Que showed the highest inhibition rate of 44.64% ($p < 0.05$), indicating that it was the most effective candidate for reducing IgE recognition of gliadin. This stronger inhibitory effect may be partly explained by the favorable hydroxyl distribution and planar flavonol structure of Que. Que contains five hydroxyl groups at C3, C5, C7, C3′, and C4′, together with a C2=C3 double bond and a 4-oxo group, providing multiple hydrogen-bonding sites and an extended conjugated surface for interaction with gliadin [24]. In contrast, caffeic acid has only

462 one aromatic ring with two phenolic hydroxyl groups, chlorogenic acid contains a
463 bulky quinic acid moiety that may hinder hydroxyl accessibility, and catechin has a
464 non-planar flavan-3-ol skeleton, which may limit effective binding orientation. These
465 structural features may promote hydrogen bonding, hydrophobic interactions, and van
466 der Waals forces between Que and gliadin, leading to conformational rearrangement
467 and reduced epitope accessibility, thereby reducing IgE recognition [25].

468 As shown in Fig. 1B, HHP treatment also significantly affected the IgE-binding
469 capacity of gliadin ($p < 0.05$). With increasing pressure, the relative IgE-binding
470 reduction initially increased and then decreased, suggesting that moderate pressure
471 promoted a favorable conformational rearrangement, whereas excessive pressure
472 might cause structural reaggregation or re-exposure of IgE-accessible regions. HHP is
473 known to disrupt non-covalent interactions, induce partial unfolding, expose buried
474 hydrophobic domains, and modify protein aggregation behavior, thereby changing
475 epitope accessibility and immunoreactivity [9]. In wheat gluten systems, the
476 allergenicity-reducing effect of HHP has also been reported to be pressure-dependent
477 rather than linearly enhanced with increasing pressure [10]. Accordingly, 500 MPa
478 produced the highest IgE-binding inhibition and was selected as the optimal pressure
479 level for subsequent experiments.

480 The effect of treatment sequence was further evaluated (Fig. 1C). Compared with
481 single HHP or quercetin treatment, the combined treatments produced a greater
482 reduction in IgE binding, indicating a synergistic or complementary effect between
483 pressure-induced structural remodeling and quercetin-mediated complex formation.

Notably, Gli-HHP-Que showed a higher inhibition rate than Gli-Que-HHP, suggesting that the order of HHP and quercetin application was a key determinant of gliadin immunoreactivity reduction. This result supports the hypothesis that HHP pretreatment first loosens the gliadin structure and increases the accessibility of potential quercetin-binding regions, thereby facilitating subsequent quercetin binding and further limiting IgE epitope exposure [26].

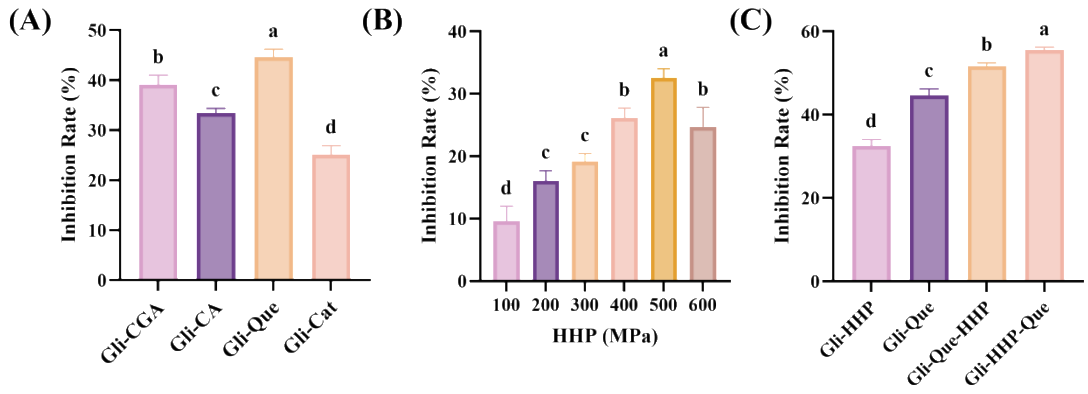


Fig. 1. Effects of different treatments on the relative IgE-binding reduction of gliadin.

(A) Effect of polyphenol type. (B) Effect of HHP pressure level. (C) Effect of HHP, quercetin, and different treatment sequences. Different letters indicate significant differences between data points ($p < 0.05$).

3.2 Structural and physicochemical characterization

As shown in Fig. 2A, native gliadin showed major bands around 30-35 kDa, mainly corresponding to the α/β-gliadin fraction [27]. No obvious low-molecular-weight degradation bands appeared after HHP treatment, indicating that pressure treatment did not visibly cleave gliadin peptide chains under the present conditions [28]. In the quercetin-containing groups, the bands were slightly intensified and showed a subtle

shift toward the higher-molecular-weight region, which was consistent with gliadin-quercetin complex formation or limited aggregate formation [25].

The CD, UV absorption, and intrinsic fluorescence spectra collectively reflected treatment-induced changes in the secondary and tertiary structures of gliadin (Fig. 2B-D). In the CD spectra, the characteristic gliadin signals were retained, but the treated groups showed clear changes in ellipticity and spectral profiles, indicating rearrangement of secondary structure rather than complete structural destruction. Meanwhile, HHP increased the exposure of chromophoric and aromatic groups, suggesting that pressure disrupted weak non-covalent interactions and loosened the compact gliadin structure, thereby exposing previously buried aromatic and hydrophobic regions instead of breaking the peptide backbone [25,28].

Compared with HHP alone, the quercetin-containing groups exhibited obvious fluorescence quenching, especially Gli-HHP-Que, indicating that quercetin changed the local environment of aromatic residues in gliadin. This effect is likely related to the hydroxyl groups and planar conjugated structure of quercetin, which favor hydrogen bonding, hydrophobic interactions, van der Waals forces, and possibly oxidation-related covalent binding with gliadin [29-32]. The stronger spectral changes observed in Gli-HHP-Que therefore suggest that HHP pretreatment enhanced the subsequent interaction between quercetin and gliadin.

Surface hydrophobicity and free sulfhydryl content further supported the structural remodeling of gliadin (Fig. 2E-F). Gli-HHP showed a pronounced increase in surface hydrophobicity, indicating that HHP-induced unfolding exposed previously

buried hydrophobic domains. Meanwhile, the increased free sulfhydryl content after HHP treatment suggested that pressure processing may disrupt or rearrange part of the disulfide bonds in gliadin, thereby releasing more detectable sulfhydryl groups [33]. In the quercetin-containing groups, the elevated free sulfhydryl content may be associated with the reducing capacity of quercetin, which could modulate the thiol-disulfide balance and maintain more sulfhydryl groups in a detectable reduced state [34]. In the combined-treatment groups, HHP-induced unfolding may further facilitate sulfhydryl exposure and quercetin-mediated redox remodeling. These results indicate sulfhydryl release/exposure and redox-related structural rearrangement rather than extensive peptide-chain cleavage.

Particle size and zeta-potential results showed that the treated samples generally had smaller particle sizes and higher absolute zeta-potential values, with the most pronounced changes observed in Gli-HHP-Que (Fig. 2G). This indicates that HHP promoted partial disassembly of large gliadin aggregates, while subsequent quercetin binding helped stabilize the remodeled particles by modifying surface charge distribution and limiting disordered reaggregation [25,28,35]. Thus, Gli-HHP-Que did not simply undergo nonspecific unfolding, but formed a smaller and more stable dispersed composite system [9].

Overall, these results support a sequence-dependent two-step remodeling mechanism. HHP first loosened gliadin aggregates by disrupting non-covalent interactions and exposing internal aromatic, hydrophobic, and sulfhydryl-containing regions; subsequent quercetin addition then interacted with these exposed sites and

reorganized the protein surface. This HHP-facilitated quercetin binding likely reduced epitope accessibility and provides a structural explanation for the stronger decrease in IgE-binding capacity observed in Gli-HHP-Que.

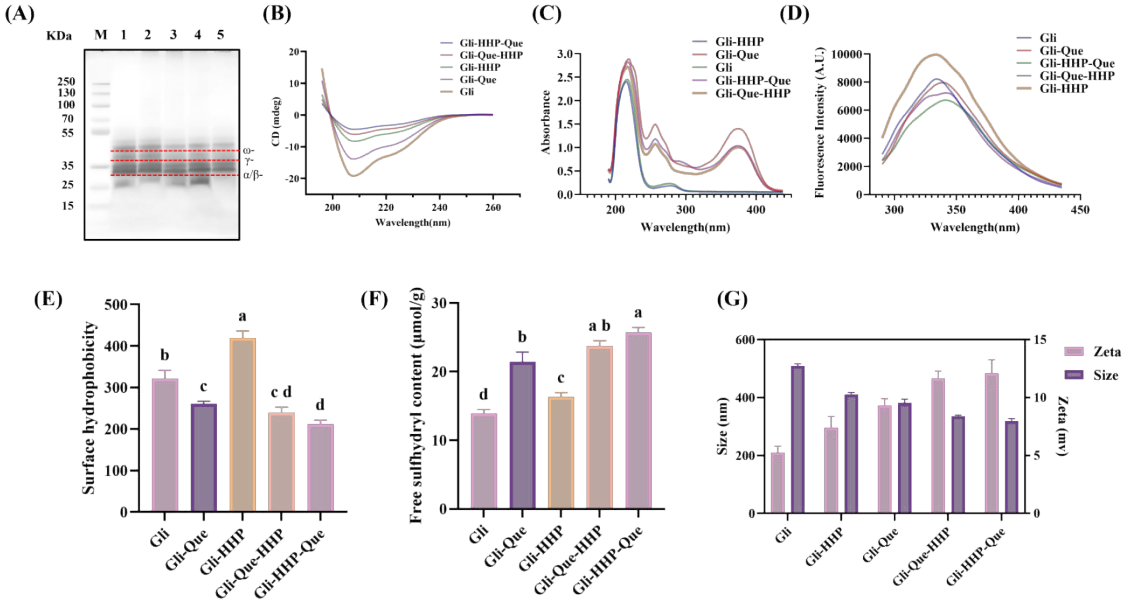


Fig. 2. Structural and physicochemical characterization of gliadin after HHP and quercetin treatments.

(A) SDS-PAGE patterns of native and treated gliadin samples. M, protein marker; lanes 1-5 represent Gli, Gli-Que, Gli-HHP, Gli-Que-HHP, and Gli-HHP-Que, respectively. (B) Far-UV circular dichroism spectra. (C) UV-Vis absorption spectra. (D) Intrinsic fluorescence spectra. (E) Surface hydrophobicity. (F) Free sulfhydryl content. (G) Particle size and zeta potential. Different letters indicate significant differences between data points ($p < 0.05$).

3.3 Simulated digestion and post-digestion immunoreactivity

Simulated gastrointestinal digestion was performed to determine whether the treatments affected the degree of hydrolysis of gliadin and the IgE-binding capacity of the resulting digestion products. As shown in Fig. 3A, the relative IgE-binding

562 inhibition rates of all treated groups increased after gastric digestion and further
563 increased after gastrointestinal digestion. Among the treated samples, Gli-HHP-Que
564 exhibited the highest inhibition after gastrointestinal digestion, indicating that HHP
565 pretreatment followed by quercetin addition not only reduced the IgE-binding
566 capacity of native gliadin, but also retained a stronger inhibitory effect after digestive
567 processing. The degree of hydrolysis increased progressively with digestion time
568 during both the gastric and gastrointestinal phases (Fig. 3B-C). Overall, Gli-HHP
569 showed the highest hydrolysis extent, whereas the quercetin-containing groups
570 generally showed lower hydrolysis, with Gli-Que-HHP exhibiting the lowest values
571 across most time points. This result is consistent with previous reports that HHP
572 enhances proteolytic susceptibility by loosening protein structure and exposing
573 cleavage sites [36]. In contrast, quercetin complexation may alter the conformation and
574 physicochemical properties of gliadin, thereby partially restricting enzyme
575 accessibility.

576 Notably, the trend in hydrolysis did not fully parallel the IgE-binding inhibition
577 results, suggesting that post-digestion immunoreactivity was not determined solely by
578 the overall degree of hydrolysis. This may be related to the mismatch between the
579 cleavage specificity of trypsin and the sequence characteristics of known gliadin
580 linear IgE epitopes. Trypsin preferentially cleaves after Lys and Arg residues,
581 whereas many reported gliadin IgE-binding motifs, such as QQX1PX2QQ,
582 QPQQPFP, QQQPP, QQIPQQQ, and QQFPQQQ, are rich in Gln and Pro but contain
583 few or no Lys/Arg sites. Therefore, the stronger post-digestion inhibition observed in

Gli-HHP-Que was more likely associated with pressure-induced changes in digestive behavior together with quercetin-assisted remodeling or masking of epitope-containing regions [37,38]. Overall, HHP mainly promoted gliadin hydrolysis, whereas subsequent quercetin-mediated complex formation further contributed to the reduction in the IgE-binding capacity of digestion products. These results indicate that HHP pretreatment followed by quercetin addition was more effective in attenuating post-digestion immunoreactivity. Because overall hydrolysis alone could not fully explain the differences in post-digestion IgE binding, peptide-level analysis of epitope-containing regions was further required.

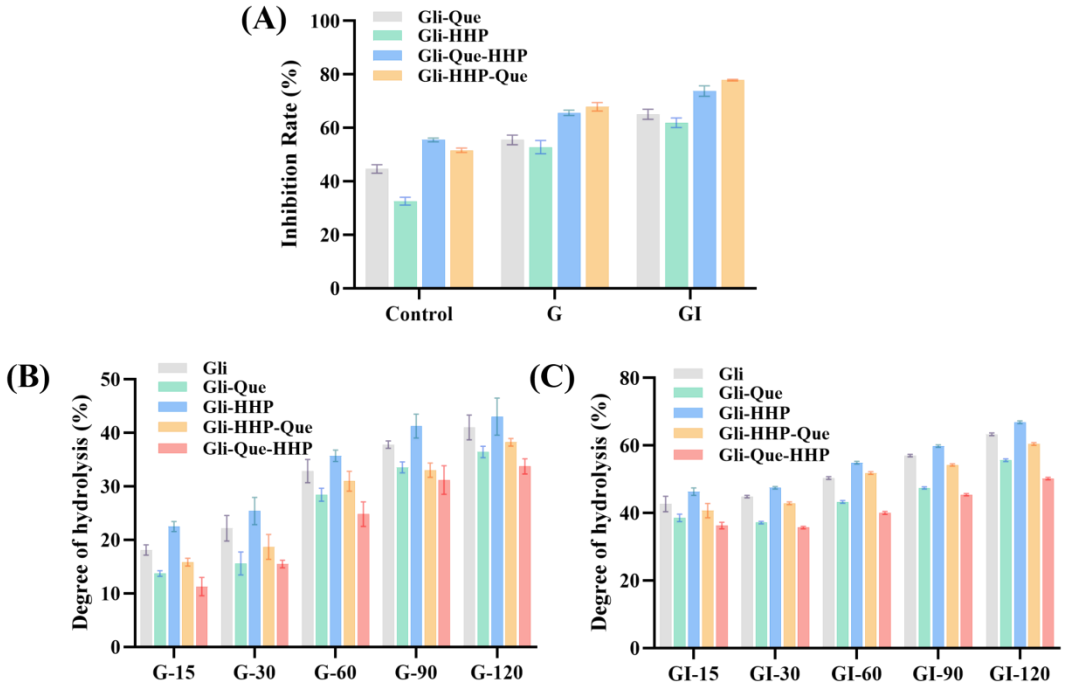


Fig. 3. Changes in relative IgE-binding reduction and digestibility of gliadin samples during simulated digestion.

(A) IgE-binding inhibition rate of different gliadin samples before digestion, after simulated gastric digestion (G), and after simulated gastrointestinal digestion (GI). (B) Degree of

hydrolysis of gliadin samples during simulated gastric digestion at 15, 30, 60, 90, and 120 min. (C) Degree of hydrolysis of gliadin samples during simulated gastrointestinal digestion at 15, 30, 60, 90, and 120 min.

3.4 Epitope-resolved peptide responses revealed by targeted proteomics

PRM-based targeted proteomics was used to further determine whether the structural remodeling induced by HHP and quercetin was linked to changes in linear allergenic epitope-containing peptides. As shown in Fig. 4, the abundance of most quantified epitope-containing peptides decreased after combined treatment. Compared with native gliadin, 19 epitope-containing peptides decreased in Gli-Que-HHP, whereas 21 decreased in Gli-HHP-Que, indicating that both treatment sequences reduced the detectable abundance of linear allergenic epitopes. Notably, Gli-HHP-Que produced a greater overall reduction, suggesting that HHP pretreatment before quercetin addition was more effective in decreasing the abundance and potential accessibility of epitope-containing peptides.

Several Pro/Gln-rich epitope-related peptides, including PHQPQQQFPQPQQPQQQF, QQILQQQLIPCRD, QQCCQQLAQIPQQL, PQQPYPSQQPY, and NMQVDPSSQVQWPQQQPVPQPHQPF, showed obvious decreases after treatment. These sequences are located in typical gliadin epitope-rich regions, which are closely associated with IgE recognition in wheat allergy [39,40]. Structural mapping further showed that some of the most responsive peptides were located close to the predicted quercetin-binding region. This spatial correspondence

supports the possibility that local quercetin binding altered the microenvironment of nearby epitope regions, thereby reducing their accessibility or changing their detectable peptide yield during PRM analysis.

The PRM results also showed that not all epitope-containing peptides responded uniformly. A few peptides, such as ALQTLPAMCNVY and QPSQLNPQAQGSVQPQQLPQFAEIR, showed slight increases or limited changes after treatment. This indicates that the effect of HHP-assisted quercetin modification was site-dependent rather than a nonspecific decrease in all peptides. The different responses among epitope peptides may be related to their local conformation, subunit origin, amino acid composition, and distance from the quercetin-binding region. Therefore, the decrease in epitope peptide abundance, together with structural mapping, these site-dependent peptide responses provide epitope-resolved evidence that the sequence-dependent structural remodeling of gliadin was accompanied by selective changes in the detectable abundance of putative epitope-containing regions. Together with the structural characterization and molecular simulation results, the PRM data further support the greater effect of Gli-HHP-Que. HHP pretreatment promoted quercetin accommodation and stabilized the gliadin-quercetin complex, which was accompanied by a greater overall decrease in the detectable abundance of putative epitope-containing peptides.

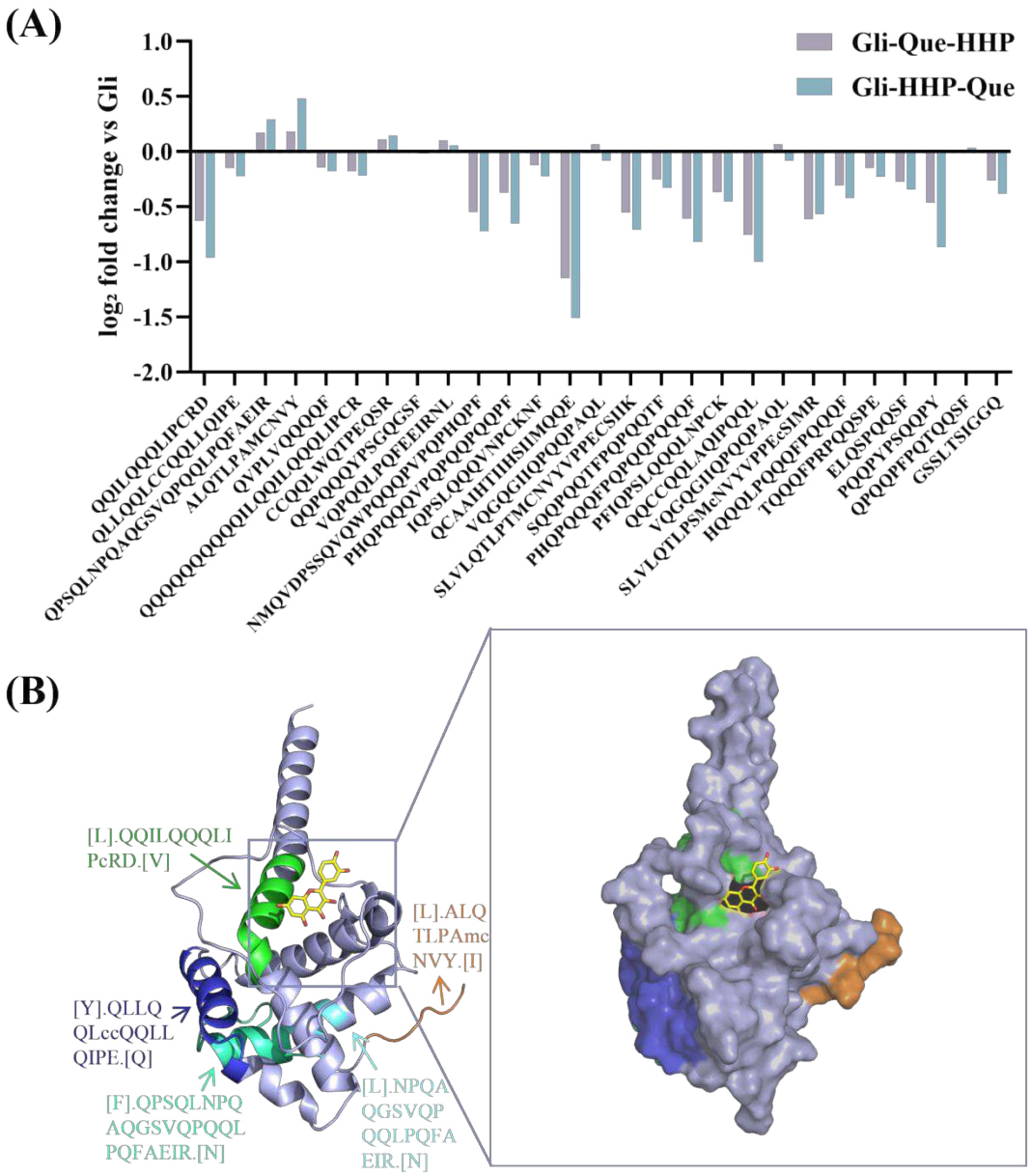


Fig. 4. Integration of PRM-based linear epitope changes and quercetin-binding site in α-gliadin.

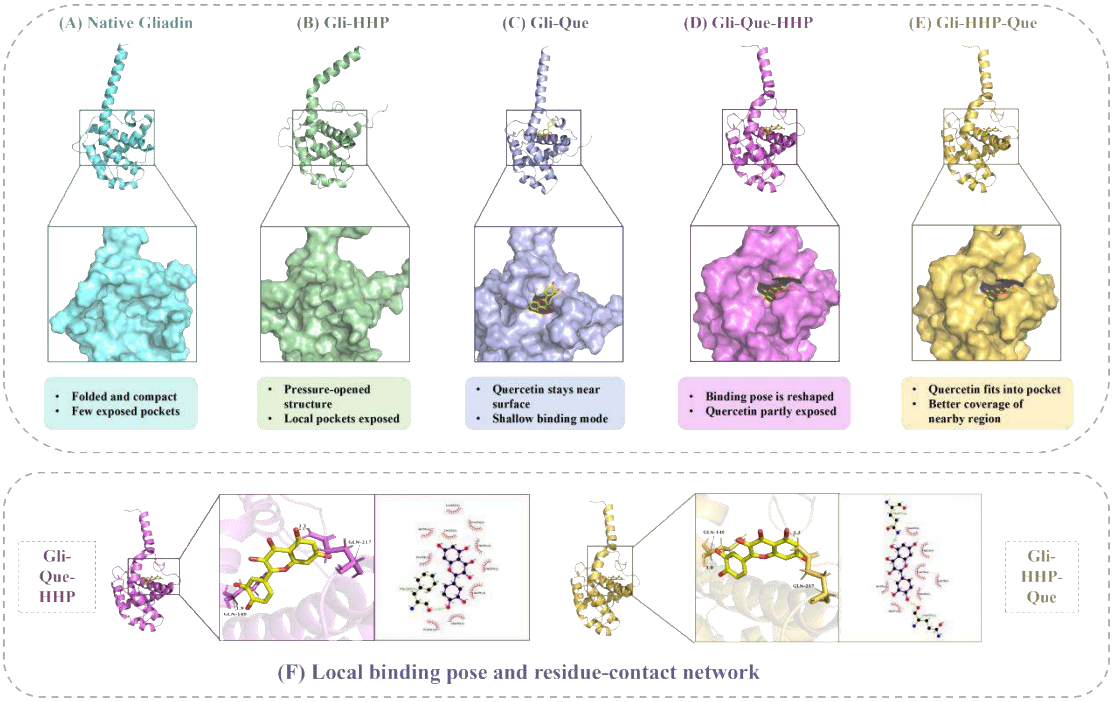
(A) Log_2 fold changes of representative epitope-containing peptides in Gli-Que-HHP and Gli-HHP-Que relative to native gliadin. (B) Structural mapping of representative epitope-related peptides on α-gliadin and their spatial relationship with quercetin.

3.5 Molecular docking and molecular dynamics simulations

To clarify the structural basis of the sequence-dependent reduction in gliadin immunoreactivity, molecular docking and molecular dynamics (MD) simulations were performed to compare quercetin-binding behavior under different processing sequences. As shown in Fig. 5, native gliadin displayed a relatively compact conformation, in which several potential binding cavities were partially buried. After HHP treatment, the gliadin structure became locally loosened, exposing additional surface pockets. When quercetin was directly introduced into native gliadin, it was mainly located near the protein surface, suggesting a relatively shallow binding mode. In contrast, HHP pretreatment allowed quercetin to be accommodated more deeply within the exposed pocket and to form closer local contacts with surrounding residues. This indicates that HHP did not simply disrupt gliadin structure, but created a more accessible conformational state for subsequent quercetin binding. Similar high-pressure-assisted modulation of food protein-polyphenol binding has been reported in β-lactoglobulin systems, where pressure-induced structural changes altered polyphenol-binding behavior and complex stability[41].

A clear difference was also observed between the two combined treatment sequences. In the Gli-Que-HHP system, the preformed gliadin-quercetin complex was further reshaped by pressure, and quercetin remained partly exposed at the protein surface. By contrast, in the Gli-HHP-Que system, pressure-induced structural loosening occurred before ligand binding, allowing quercetin to fit into a more suitable local pocket. The enlarged binding-site view and two-dimensional residue-contact network further suggested that Gli-HHP-Que formed a more compact

669 ligand-residue interaction pattern than Gli-Que-HHP. This suggests that the treatment
670 sequence affected not only the overall conformation of gliadin, but also the final
671 spatial position and potential shielding capacity of quercetin around the binding
672 region.



673

674 **Fig. 5. Molecular docking-based visualization of gliadin conformational remodeling and**
675 **quercetin-binding behavior after different treatments.**

676 (A-E) Representative conformations and surface structures of native and treated gliadin. (F)
677 Local binding conformation and residue-contact network of quercetin in Gli-Que-HHP and
678 Gli-HHP-Que.

679

680 MD simulations further supported the sequence-dependent stabilization of the
681 gliadin-quercetin complex (Fig. 6). The RMSD profiles showed that Gli-HHP-Que
682 exhibited the smallest fluctuation and reached equilibrium more rapidly, indicating
683 higher conformational stability. RMSF analysis also showed lower residue-level

flexibility in Gli-HHP-Que, suggesting the formation of a more stable binding interface [42,43]. In addition, the relatively stable Rg value of Gli-HHP-Que indicated that the complex maintained a compact conformation during the simulation. These results demonstrate that HHP pretreatment enhanced the structural compatibility between gliadin and quercetin, thereby stabilizing the resulting complex [44].

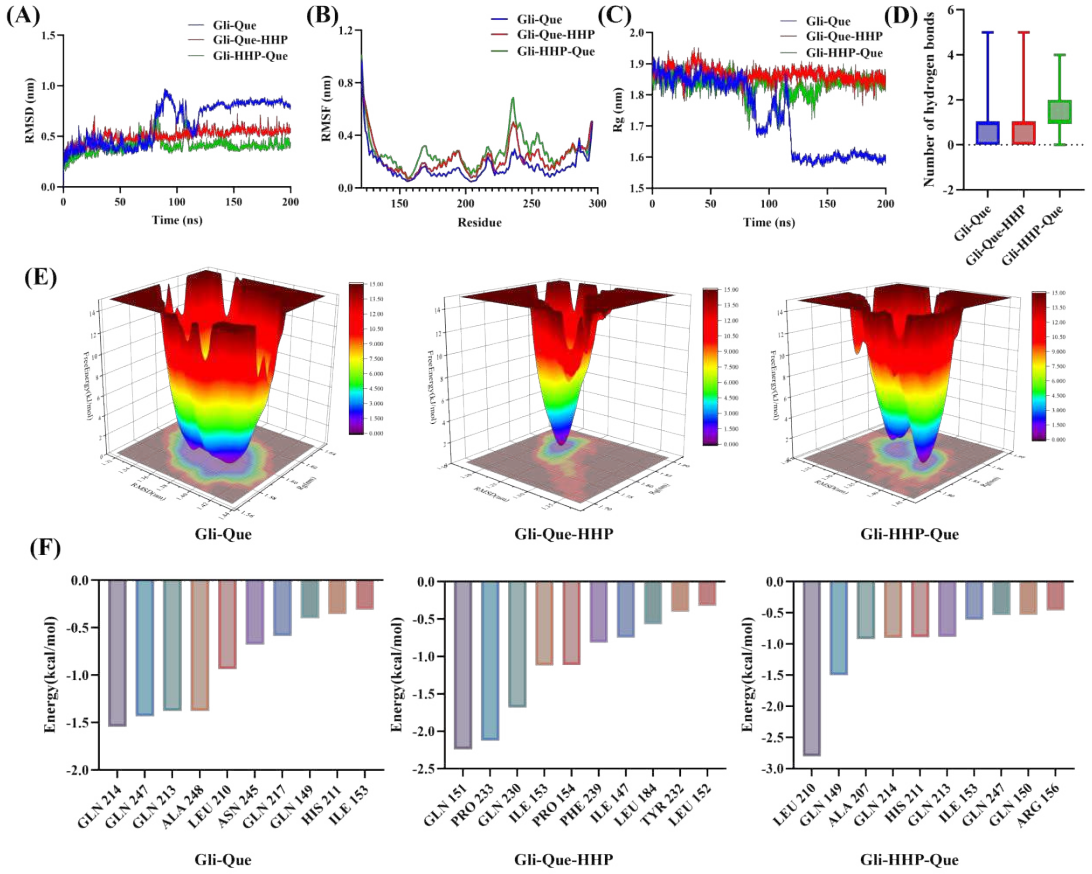


Fig. 6. Molecular dynamics simulation and binding free-energy analysis of quercetin-gliadin complexes under different processing sequences.

(A) RMSD, (B) RMSF, (C) Rg, (D) Number of hydrogen bonds, (E) Free energy landscapes of the three complexes plotted as a function of RMSD and Rg, (F) Residue-level energy contribution of key amino acid residues involved in quercetin binding.

Hydrogen bond and free energy landscape analyses provided further support for this conclusion. Gli-HHP-Que maintained a more persistent hydrogen-bonding network with smaller fluctuations, indicating stronger intermolecular interactions. Meanwhile, the free energy landscape of Gli-HHP-Que showed a more concentrated low-energy basin, suggesting that this system preferentially converged toward a stable dominant conformation. The MM/PBSA results (Table.1) showed that all gliadin-quercetin complexes had negative binding free energies, whereas Gli-HHP-Que exhibited the most favorable binding free energy (−20.18 ± 3.17 kcal/mol). Energy decomposition analysis indicated that van der Waals interactions were the major driving force, with additional contributions from electrostatic interactions, while polar solvation partially offset complex formation [45]. These results indicate that HHP pretreatment strengthened quercetin binding mainly by promoting a more favorable local binding environment.

Taken together, the molecular docking and MD results suggest that HHP pretreatment loosened the gliadin conformation, exposed potential quercetin-binding regions, and promoted the formation of a more stable gliadin-quercetin complex. This stabilized complex may reduce IgE accessibility by sterically shielding nearby epitope-containing regions and altering the digestion-derived presentation of allergenic peptides. Therefore, the lower immunoreactivity of Gli-HHP-Que may be attributed not only to stronger quercetin binding, but also to the formation of a less immunologically accessible gliadin conformation.Based on these integrated findings, HHP pretreatment followed by Que was identified as the optimal processing sequence

718 and was therefore further validated at the cellular level using serum-sensitized KU812
719 cells.
720
721 **Table 1. MM/PBSA-derived binding free energy components of gliadin-quercetin**
722 **complexes under different processing sequences.**

Energy component (kcal/mol)	Gli-Que	Gli-Que-HHP	Gli-HHP-Que
van der Waals energy	-30.45 ± 4.89	-32.67 ± 3.16	-30.71 ± 2.94
electrostatic energy	-12.17 ± 7.00	-15.62 ± 6.72	-18.18 ± 5.96
Generalized Born solvation energy	30.20 ± 5.61	34.59 ± 4.68	32.95 ± 4.30
surface area energy	-4.07 ± 0.54	-4.06 ± 0.26	-4.24 ± 0.28
gas-phase interaction energy	-42.62 ± 7.58	-48.29 ± 7.03	-48.89 ± 6.01
solvation free energy	26.13 ± 5.34	30.54 ± 4.54	28.71 ± 4.18
total binding energy	-16.49 ± 3.66	-17.76 ± 3.70	-20.18 ± 3.17

723
724 **3.6 Effects of gliadin treatments on KU812 cell viability, Ca^{2+} mobilization,**
725 **degranulation, and inflammatory mediator release**
726 Before evaluating allergenic cell activation, the cytotoxicity of native and treated
727 gliadin samples toward KU812 cells was assessed using the CCK-8 assay. As shown
728 in Fig. 7A, no obvious decrease in cell viability was observed at 0.15-0.6 mg/mL,
729 whereas cell viability declined markedly at 1.2 mg/mL. Therefore, 0.6 mg/mL was
730 selected as the working concentration for subsequent KU812 cell experiments to
731 avoid cytotoxic interference.

The effects of different gliadin samples on KU812 cell activation were further evaluated by measuring intracellular Ca^{2+} mobilization, degranulation, and inflammatory mediator release. Native gliadin markedly increased intracellular Ca^{2+} fluorescence intensity, indicating strong activation of serum-sensitized KU812 cells (Fig. 7B-C). In contrast, all treated gliadin samples reduced Ca^{2+} mobilization to different extents, with Gli-HHP-Que showing the lowest fluorescence intensity. Since Ca^{2+} mobilization is an early event in IgE/FcεRI-mediated mast cell and basophil activation, this result suggests that the treated gliadin samples had a weaker ability to initiate allergic effector-cell activation.

Consistently, native gliadin significantly increased β-hexosaminidase release, histamine secretion, and the degranulation ratio, confirming its ability to induce degranulation in serum-sensitized KU812 cells (Fig. 7D-F). β-Hexosaminidase release is commonly used as an indicator of granule exocytosis, histamine is a representative immediate allergic mediator released during mast cell/basophil activation, and the degranulation ratio reflects the overall degree of effector-cell degranulation. Compared with the Gli group, all treated gliadin samples reduced these three degranulation-related indicators, suggesting that the treatments weakened the immediate allergic response induced by gliadin. In addition, native gliadin promoted the secretion of TNF-α, IL-6, and IL-4, whereas the treated samples decreased these cytokine levels to different extents (Fig. 7G-I). TNF-α and IL-6 reflect pro-inflammatory activation, while IL-4 is closely associated with type 2 allergic inflammation and IgE-related immune responses. Among all treatment groups,

Gli-HHP-Que consistently showed the lowest levels of degranulation markers and inflammatory cytokines. These results indicate that HHP pretreatment followed by quercetin addition not only inhibited early Ca^{2+} mobilization, but also suppressed downstream degranulation and inflammatory mediator release, thereby attenuating gliadin-induced KU812 cell activation. These cellular responses were in line with the reduced IgE-binding capacity and lower detectability of epitope-containing peptides observed for Gli-HHP-Que, supporting its reduced ability to stimulate sensitized KU812 cells.

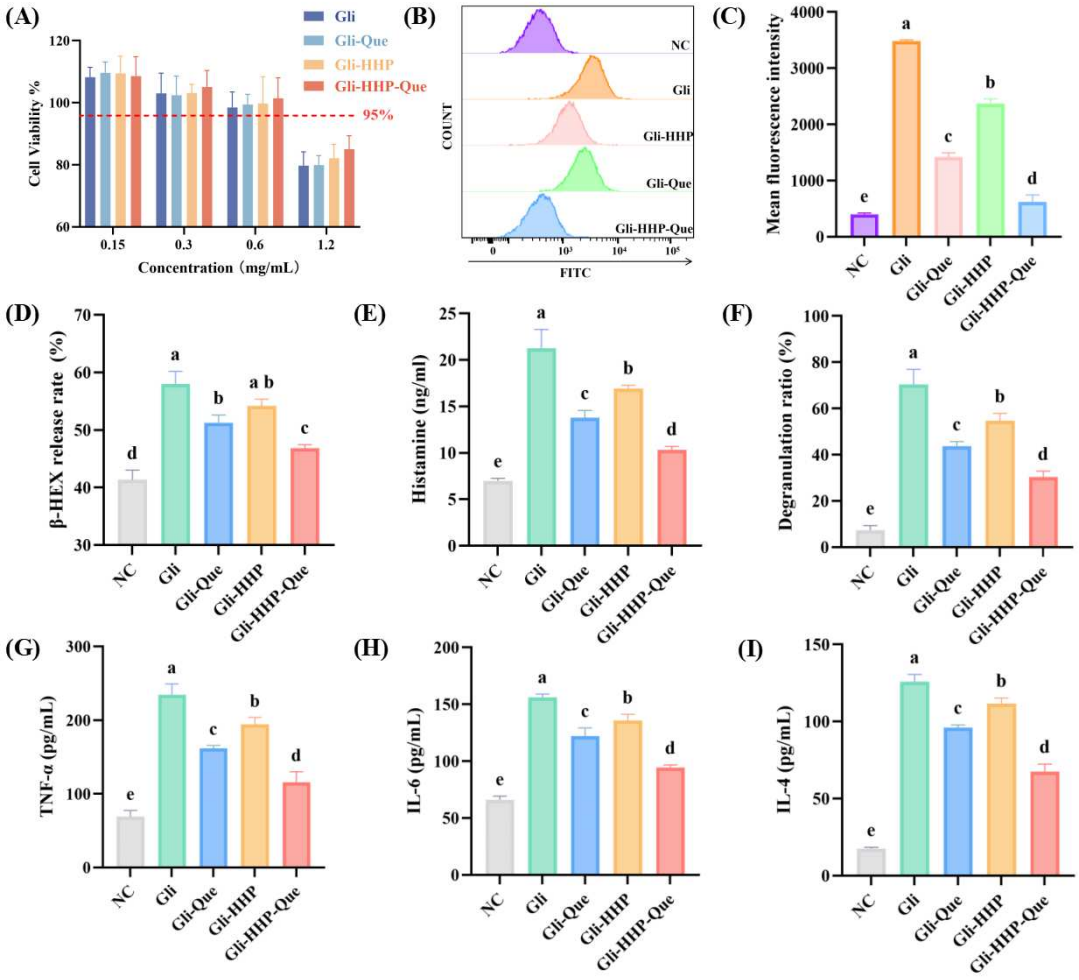


Fig. 7. Effects of different gliadin treatments on KU812 cell responses.

765 (A) Cell viability of KU812 cells. (B) Representative flow cytometry histograms of
766 intracellular Ca^{2+} levels. (C) Quantification of intracellular Ca^{2+} fluorescence intensity. (D)
767 β-Hexosaminidase release rate. (E) Histamine level. (F) Degranulation ratio. (G) TNF-α level.
768 (H) IL-6 level. (I) IL-4 level.
769
770 **3.7 Signaling pathways in KU812 cells**
771 Western blotting was further performed to clarify whether the reduced cellular
772 responses were associated with changes in IgE/FcεRI-related signaling pathways. As
773 shown in Fig. 8, native gliadin markedly increased the phosphorylation levels of Lyn,
774 Syk, and PLCγ1, whereas the corresponding total protein levels showed no significant
775 differences among groups (Fig. 8). This indicates that gliadin-induced KU812 cell
776 activation was mainly related to phosphorylation-dependent signal transduction rather
777 than changes in total protein abundance. FcεRI-mediated activation is initiated by Src
778 family kinases such as Lyn, followed by Syk activation and downstream
779 PLCγ1-dependent Ca^{2+} mobilization, which collectively contribute to degranulation
780 and mediator release [46,47]. Therefore, the increased p-Lyn/Lyn, p-Syk/Syk, and
781 p-PLCγ1/PLCγ1 ratios in the Gli group suggest that native gliadin activated the early
782 allergic signaling cascade in serum-sensitized KU812 cells.
783 Compared with the Gli group, all treated gliadin samples attenuated the
784 phosphorylation of Lyn, Syk, and PLCγ1, with Gli-HHP-Que showing the strongest
785 inhibitory effect. The greater reductions in p-Lyn, p-Syk, and p-PLCγ1 in
786 Gli-HHP-Que indicate that HHP pretreatment followed by quercetin addition more

787 effectively weakened the ability of gliadin to activate the FcεRI-associated
788 Lyn/Syk/PLCγ1 axis. This finding is consistent with the decreased Ca^{2+} mobilization
789 and degranulation-related indicators observed in the treated groups, further supporting
790 that the modified gliadin samples had reduced effector-cell stimulatory activity. The
791 stronger inhibition observed in Gli-HHP-Que may be attributed to reduced IgE
792 recognition and epitope accessibility after structural remodeling and
793 quercetin-mediated epitope shielding.

794 Downstream inflammatory signaling showed a similar trend. Native gliadin
795 increased the phosphorylation levels of ERK, JNK, p38, and NF-κB p65, indicating
796 activation of MAPK/NF-κB-related inflammatory signaling. MAPK signaling is
797 closely involved in mast cell/basophil activation, cytokine production, and allergic
798 inflammatory responses [48]. After treatment, the phosphorylation levels of these
799 downstream signaling proteins were reduced to different degrees, whereas the total
800 levels of ERK, JNK, p38, and NF-κB p65 showed no significant differences among
801 groups (Fig. 8). Among the treated groups, Gli-HHP-Que again exhibited the lowest
802 phosphorylation levels. This result agrees with the reduced secretion of TNF-α, IL-6,
803 and IL-4, suggesting that attenuation of MAPK/NF-κB signaling contributed to the
804 suppression of gliadin-induced inflammatory and allergy-related responses [49].

805 Taken together, native gliadin activated the FcεRI-associated Lyn/Syk/PLCγ1
806 axis and downstream MAPK/NF-κB signaling pathways, whereas HHP and quercetin
807 treatments weakened this activation. Among all treatments, Gli-HHP-Que produced
808 the strongest suppression of both upstream allergic signaling and downstream

inflammatory signaling. Combined with the structural, molecular simulation, PRM, and cellular functional results, these findings support the proposed mechanism that HHP pretreatment facilitates quercetin-mediated remodeling of gliadin, reduces epitope accessibility, and ultimately weakens IgE-dependent KU812 cell activation.

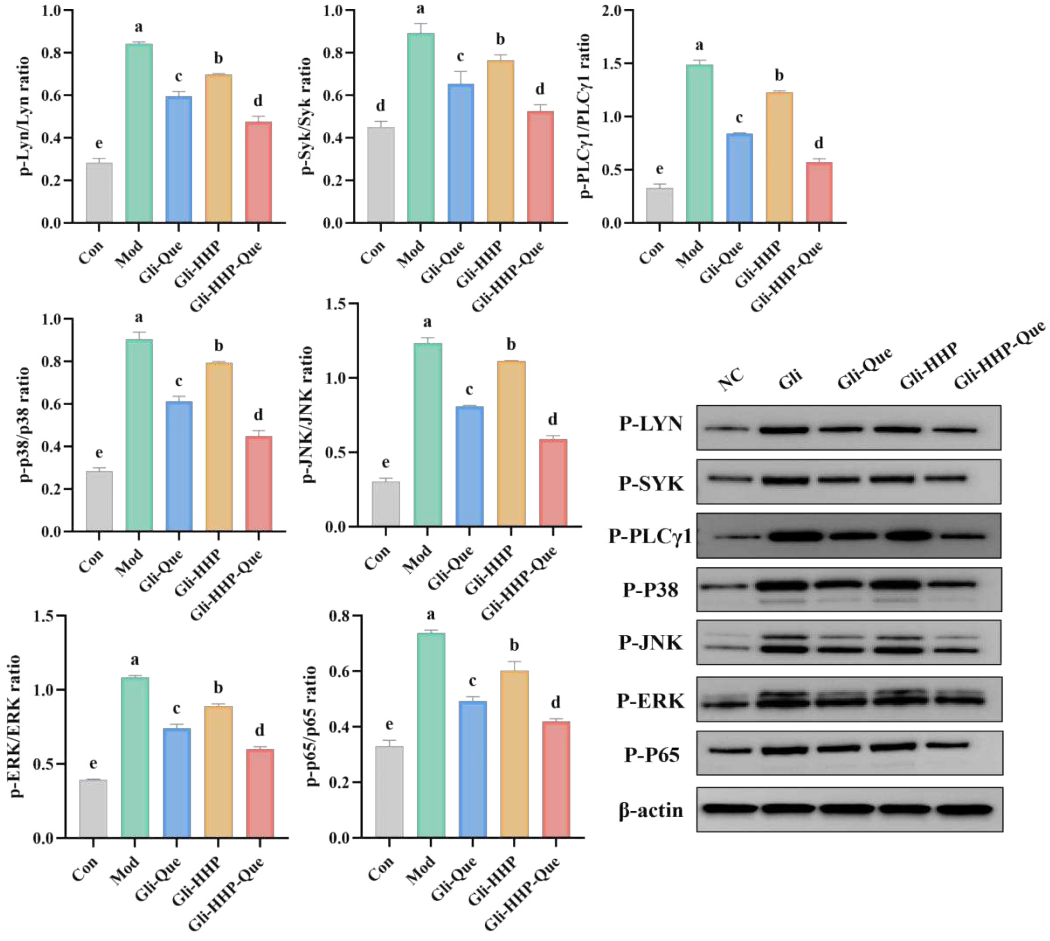


Fig. 8. Effects of different gliadin treatments on FcεRI-mediated signaling pathways in KU812 cells.

4 Conclusion

In this study, quercetin (Que) and 500 MPa were identified as the most effective polyphenol and pressure conditions, respectively, for reducing gliadin

immunoreactivity. Furthermore, HHP pretreatment followed by Que intervention was found to be the superior processing sequence, leading to a further significant reduction in IgE-binding capacity, with this advantage retained after simulated gastrointestinal digestion. Protein structural characterization and molecular dynamics simulations further revealed that HHP pretreatment-induced conformational relaxation of gliadin facilitated enhanced Que binding, with the binding domains located in proximity to the linear epitope regions of gliadin. PRM analysis further showed that this sequence was accompanied by a greater overall decrease in the detectable abundance of putative epitope-containing peptides. At the cellular level, Gli-HHP-Que more effectively inhibited Ca^{2+} mobilization, degranulation, and inflammatory mediator release in serum-sensitized KU812 cells, together with attenuation of the FcεRI-associated Lyn/Syk/PLCγ1 axis and downstream MAPK/NF-κB signaling. These cellular responses were consistent with the reduced IgE recognition and epitope accessibility observed after structural remodeling. The proposed sequence-dependent mechanism is summarized in Figure 9. Collectively, the combined treatment of HHP and Que represents a feasible strategy for reducing gliadin allergenic potential, and the sequence of these two processing steps is critical to the efficacy of immunoreactivity reduction. Future studies should further validate these effects in animal models and food matrices to determine their in vivo relevance and practical applicability. These findings provide a novel and viable strategy for developing wheat-based products with reduced allergenic potential.

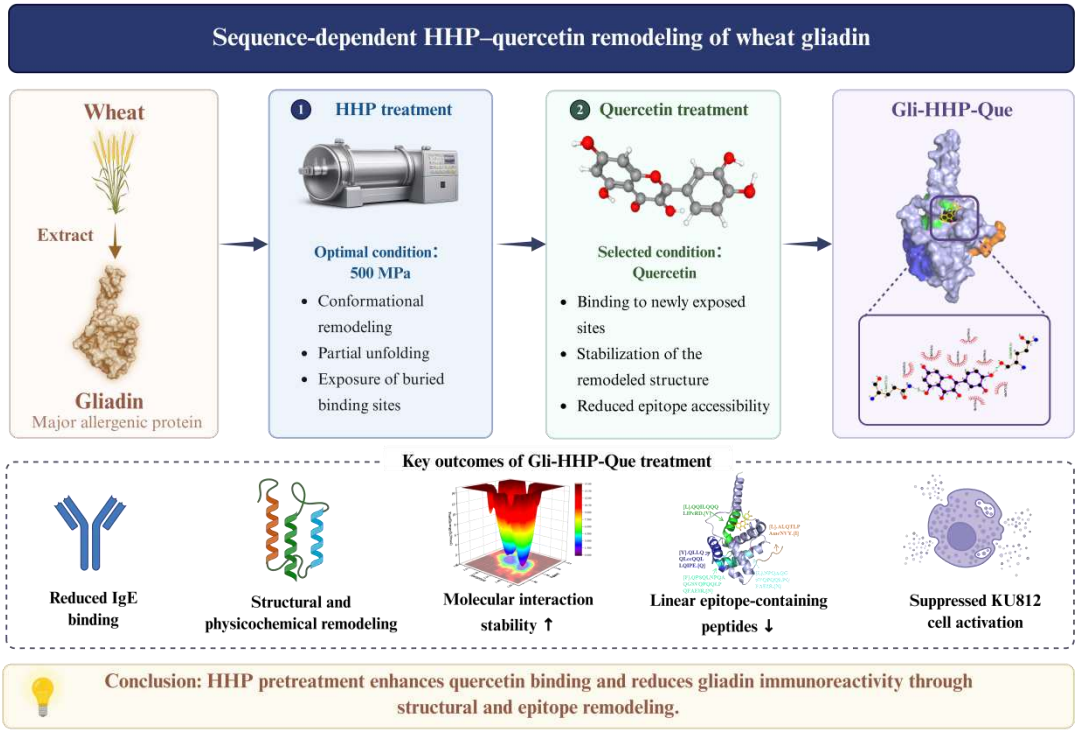


Fig. 9. Proposed mechanism for the sequence-dependent reduction of wheat gliadin immunoreactivity by high hydrostatic pressure pretreatment followed by quercetin addition.

Author Contributions

Weiman Gao: Conceptualization, Methodology, Investigation, Data curation, Formal analysis, Visualization, Writing-original draft. **Lining Ren:** Methodology, Investigation, Validation. **Xinyu Ma:** Formal analysis, Validation, Writing-review & editing. **Yuhang Xiao:** Software, Data curation, Formal analysis. **Shijing Jiang:** Formal analysis, Validation, Visualization, Writing-review & editing. **Aidong Sun:** Conceptualization, Supervision, Project administration, Funding acquisition, Writing-review & editing.

Declaration of competing interest

The authors declare that they have no known competing financial interests or personal relationships that could have appeared to influence the work reported in this paper.

Funding

This work was supported by the funding from National Natural Science Foundation of China (Grant No. 32172222 and No. 31871817).

Data availability

Data will be made available on request.

References

1 Jiang, N. *et al.* Allergens from wheat and wheat products: A comprehensive review on allergy mechanisms and modifications. *Food Chemistry: X*, 102871 (2025).

2 Balakireva, A. V. & Zamyatnin Jr, A. A. Properties of gluten intolerance: gluten structure, evolution, pathogenicity and detoxification capabilities. *Nutrients* **8**, 644 (2016).

3 Battais, F. *et al.* Identification of IgE-binding epitopes on gliadins for patients with food allergy to wheat. *Allergy* **60**, 815-821 (2005).

4 Cho, K. *et al.* Proteomic profiling and epitope analysis of the complex α-, γ-, and ω-gliadin families in a commercial bread wheat. *Frontiers in Plant Science* **9**, 818 (2018).

5 Deng, H. *et al.* From Source to Structure: Industrial Processing Technologies for Attenuating the Allergenicity of Food Proteins. *Food and Bioprocess Technology* **19**, 205, doi:10.1007/s11947-026-04285-2 (2026).

6 Arteaga-Marin, S. *et al.* Non-Thermal Food Processing for Plant Protein Allergenicity Reduction: A Systematic Review. *Food Science & Nutrition* **13**, e70430 (2025).

7 Pi, X., Sun, Y., Cheng, J., Fu, G. & Guo, M. A review on polyphenols and their potential application to reduce food allergenicity. *Critical reviews in food science and nutrition* **63**, 10014-10031 (2023).

8 Yang, J., Kumar, N., Kuang, H., Song, J. & Li, Y. Changes of digestive stability and potential allergenicity of high hydrostatic pressure-treated ovalbumin during in vitro digestion. *Food Chemistry* **473**, 142962, doi:https://doi.org/10.1016/j.foodchem.2025.142962 (2025).

9 Braspaiboon, S. & Laokuldilok, T. High Hydrostatic Pressure: Influences on Allergenicity, Bioactivities, and Structural and Functional Properties of Proteins from Diverse Food Sources. *Foods* **13**, 922 (2024).

10 Yao, Y., Jia, Y., Lu, X. & Li, H. Release and conformational changes in allergenic proteins from wheat gluten induced by high hydrostatic pressure. *Food Chemistry* **368**, 130805, doi:https://doi.org/10.1016/j.foodchem.2021.130805 (2022).

11 Pan, T. g., Wu, Y. n., He, S., Wu, Z. & Jin, R. Food allergenic protein conjugation with plant polyphenols for allergenicity reduction. *Current Opinion in Food Science* **43**, 36-42 (2022).

12 He, W. *et al.* Modulating the allergenicity and functional properties of peanut protein by covalent conjugation with polyphenols. *Food Chemistry* **415**, 135733, doi:https://doi.org/10.1016/j.foodchem.2023.135733 (2023).

13 Zhou, E. *et al.* Covalent conjugation with quercetin mitigates allergenicity of the bee pollen allergen Bra c p in a murine model. *Food Chemistry* **436**, 137722, doi:https://doi.org/10.1016/j.foodchem.2023.137722 (2024).

14 Günal-Köroğlu, D. *et al.* Allergenicity of Alternative Proteins: Reduction Mechanisms and Processing Strategies. *Journal of Agricultural and Food Chemistry* **73**, 7522-7546, doi:10.1021/acs.jafc.5c00948 (2025).

15 Zhang, K. *et al.* Effect of covalent conjugation with chlorogenic acid and luteolin on allergenicity and functional properties of wheat gliadin. *Journal of Cereal Science* **106**, 103484, doi:https://doi.org/10.1016/j.jcs.2022.103484 (2022).

16 Tsurunaga, Y., Arima, S., Kumagai, S. & Morita, E. Low Allergenicity in Processed Wheat Flour Products Using Tannins from Agri-Food Wastes. *Foods* **12**, 2722 (2023).

17 Lai, X. *et al.* Interactions between proteins and polyphenols in plant-based food: Insight of allergenicity and off-flavor reduction. *Food Chemistry* **495**, 146333, doi:https://doi.org/10.1016/j.foodchem.2025.146333 (2025).

18 Lan, T. *et al.* Effect of pH values and addition sequences on the structure and emulsifying properties of soy protein isolate-lecithin-epigallocatechin gallate ternary complexes. *Int J Biol Macromol* **344**, 150559, doi:10.1016/j.ijbiomac.2026.150559 (2026).

19 Tamsen, M., Soltanizadeh, N. & Fathi, M. The impact of compound addition sequence on functional, antioxidant, and thermal properties of dielectric barrier discharge plasma-produced ternary complexes. *Food Chemistry: X* **30**, 102978, doi:https://doi.org/10.1016/j.fochx.2025.102978 (2025).

928 20 Brodkorb, A. *et al.* INFOGEST static in vitro simulation of gastrointestinal
929 food digestion. *Nature protocols* **14**, 991-1014 (2019).
930 21 Clifford, J. N. *et al.* BepiPred-3.0: Improved B-cell epitope prediction using
931 protein language models. *Protein Science* **31**, e4497,
932 doi:https://doi.org/10.1002/pro.4497 (2022).
933 22 Saha, S. & Raghava, G. P. S. Prediction of continuous B-cell epitopes in an
934 antigen using recurrent neural network. *Proteins: Structure, Function, and*
935 *Bioinformatics* **65**, 40-48, doi:https://doi.org/10.1002/prot.21078 (2006).
936 23 Dhanda, S. K. *et al.* IEDB-AR: immune epitope database—analysis resource
937 in 2019. *Nucleic Acids Research* **47**, W502-W506, doi:10.1093/nar/gkz452
938 (2019).
939 24 Krekora, M. & Nawrocka, A. Interactions of gliadins with flavonoids and their
940 glycosides studied with application of FT-Raman spectroscopy. *Journal of*
941 *Cereal Science* **117**, 103915, doi:https://doi.org/10.1016/j.jcs.2024.103915
942 (2024).
943 25 Wang, Q. *et al.* Interaction between wheat gliadin and quercetin under
944 different pH conditions analyzed by multi-spectroscopy methods.
945 *Spectrochimica Acta Part A: Molecular and Biomolecular Spectroscopy* **229**,
946 117937, doi:https://doi.org/10.1016/j.saa.2019.117937 (2020).
947 26 Zhang, W. *et al.* Effects of high pressure processing on structural changes,
948 aggregation, and binding mechanisms of β-Lactoglobulin with typical

polyphenols. *Food Chemistry* **458**, 140265, doi:https://doi.org/10.1016/j.foodchem.2024.140265 (2024).

27 Nadeem, M. *et al.* Electrophoretic Characteristics of Gluten Proteins as Influenced by Crop Year and Variety. *International Journal of Food Properties* **19**, 897-910, doi:10.1080/10942912.2015.1045518 (2016).

28 Zhang, Y. *et al.* Effect of high hydrostatic pressure treatment on the structure and physicochemical properties of millet gliadin. *Lwt* **154**, 112755 (2022).

29 He, W. J. *et al.* Gliadin interacted with tea polyphenols: potential application and action mechanism. *Int J Food Sci Nutr* **73**, 786-799, doi:10.1080/09637486.2022.2078283 (2022).

30 Zhang, Y. *et al.* Changes on the conformational and functional properties of soybean protein isolate induced by quercetin. *Frontiers in Nutrition* **9**, 966750 (2022).

31 Kim, W., Wang, Y. & Selomulya, C. Emerging technologies to improve plant protein functionality with protein-polyphenol interactions. *Trends in Food Science & Technology* **147**, 104469, doi:https://doi.org/10.1016/j.tifs.2024.104469 (2024).

32 Sun, X., Sarteshnizi, R. A. & Udenigwe, C. C. Recent advances in protein–polyphenol interactions focusing on structural properties related to antioxidant activities. *Current Opinion in Food Science* **45**, 100840, doi:https://doi.org/10.1016/j.cofs.2022.100840 (2022).

33 Liu, H. *et al.* Effects of High Hydrostatic Pressure on the Conformational Structure and Gel Properties of Myofibrillar Protein and Meat Quality: A Review. *Foods* **10**, doi:10.3390/foods10081872 (2021).

34 Cheng, J., Xiang, R., Tang, D., Zhu, M. & Liu, X. Regulation of protein oxidation in Cantonese sausages by rutin, quercetin and caffeic acid. *Meat Sci* **175**, 108422, doi:10.1016/j.meatsci.2020.108422 (2021).

35 Li, M. *et al.* Recent Progress on Protein-Polyphenol Complexes: Effect on Stability and Nutrients Delivery of Oil-in-Water Emulsion System. *Frontiers in Nutrition* **Volume 8 - 2021**, doi:10.3389/fnut.2021.765589 (2021).

36 Wang, W. *et al.* Effect of high hydrostatic pressure processing on the structure, functionality, and nutritional properties of food proteins: A review. *Comprehensive Reviews in Food Science and Food Safety* **21**, 4640-4682, doi:https://doi.org/10.1111/1541-4337.13033 (2022).

37 Aksoy, M., Hamzalıoğlu, A. & Gökmen, V. Investigating the Formation of In Vitro Immunogenic Gluten Peptides after Covalent Modification of Their Structure with Green Tea Phenolic Compounds under Alkaline Conditions. *Journal of Agricultural and Food Chemistry* **72**, 13898-13905, doi:10.1021/acs.jafc.4c00334 (2024).

38 Sun, N. *et al.* Gastrointestinal fate of food allergens and its relationship with allergenicity. *Comprehensive Reviews in Food Science and Food Safety* **21**, 3376-3404, doi:https://doi.org/10.1111/1541-4337.12989 (2022).

991 39 Wieser, H., Koehler, P. & Scherf, K. A. Chemistry of wheat gluten proteins:
992 Qualitative composition. *Cereal Chemistry* **100**, 23-35 (2023).
993 40 Morita, E. *et al.* A narrative mini review on current status of hypoallergenic
994 wheat development for IgE-mediated wheat allergy, wheat-dependent
995 exercise-induced anaphylaxis. *Foods* **12**, 954 (2023).
996 41 Huang, Y., Zhang, X. & Suo, H. Interaction between β-lactoglobulin and
997 EGCG under high-pressure by molecular dynamics simulation. *PLoS One* **16**,
998 e0255866 (2021).
999 42 Chen, L. *et al.* Effects of different phenolic compounds on the interfacial
1000 behaviour of casein and the action mechanism. *Food Research International*
1001 **162**, 112110, doi:https://doi.org/10.1016/j.foodres.2022.112110 (2022).
1002 43 Feng, Z.-J., Xu, Q.-D., Chen, N. & Zeng, W.-C. Effects and structure-activity
1003 relationship of phenolic compounds with different structures on the
1004 physicochemical properties of casein and its action mechanism. *Food*
1005 *Hydrocolloids* **169**, 111606,
1006 doi:https://doi.org/10.1016/j.foodhyd.2025.111606 (2025).
1007 44 Baruah, I., Kashyap, C., Guha, A. K. & Borgohain, G. Insights into the
1008 Interaction between Polyphenols and β-Lactoglobulin through Molecular
1009 Docking, MD Simulation, and QM/MM Approaches. *ACS Omega* **7**,
1010 23083-23095, doi:10.1021/acsomega.2c00336 (2022).
1011 45 Valdés-Tresanco, M. S., Valdés-Tresanco, M. E., Valiente, P. A. & Moreno, E.
1012 gmx_MMPBSA: A New Tool to Perform End-State Free Energy Calculations

with GROMACS. *J Chem Theory Comput* **17**, 6281-6291, doi:10.1021/acs.jctc.1c00645 (2021).

46 Kawakami, Y. *et al.* Regulation of Syk activity by antiviral adaptor MAVS in FcεRI signaling pathway. *Frontiers in Allergy* **4**, 1098474 (2023).

47 Rana, T. S., Bansode, R. R. & Williams, L. L. Anti-Allergic and Anti-Inflammatory Signaling Mechanisms of Natural Compounds/Extracts in In Vitro System of RBL-2H3 Cell: A Systematic Review. *Cells* **13**, doi:10.3390/cells13161389 (2024).

48 Chang, T.-M., Hsiao, T.-C., Yang, T.-Y. & Huang, H.-C. IgE-induced mast cell activation is suppressed by dihydromyricetin through the inhibition of NF-κB signaling pathway. *Molecules* **26**, 3877 (2021).

49 Conte, M. *et al.* Gliadin peptide P31-43 induces mTOR/NFkβ activation and reduces autophagy: the role of lactobacillus paracasei CBA L74 postbiotc. *International journal of molecular sciences* **23**, 3655 (2022).

Supplementary Files

This is a list of supplementary files associated with this preprint. Click to download.

- SupportingInformation.docx
- Supplementaryuncroppedblot.docx